Molecular Dynamics Simulation Study on the Wetting Behavior of a Graphite Surface Textured with Nanopillars

Joyanta K. Saha, Mohammad A. Matin, Jihye Jang, and Joonkyung Jang[*]

Department of Nanomaterials Engineering, Pusan National University, Miryang 627-706, Korea. [*]E-mail: jkjang@pusan.ac.kr

Molecular dynamic simulations were performed to examine the wetting behavior of a graphite surface textured with nanoscale pillars. The contact angle of a water droplet on parallelepiped or dome-shaped pillars was investigated by systematically varying the height and width of the pillar and the spacing between pillars. An optimal inter-pillar spacing that gives the highest contact angle was found. The droplet on the dome-covered surface was determined to be more mobile than that on the surface covered with parallelepiped pillars.

Key Words : Water droplet, Superhydrophobic surface, Contact angle, Mobility

Introduction

Superhydrophobic surfaces have potential applications as water repellent glasses,[1] self -cleaning cloths[2] and low-drag marine vessels.[3] A typical superhydrophobic surface induces a high contact angle of 150° or higher for a water droplet placed on it. In addition, a superhydrophobic surface should impart high mobility to the droplet, which is characterized by a small contact angle hysteresis.[4] The hydrophobicity of a surface is enhanced dramatically by surface roughening.[5] In particular, micro- or nano- pillars endow a surface with high water repellency.[1,3,6,7] For example, the surface of a lotus leaf that is textured with hierarchical pillars (nanohairs on micropillars) induces a high contact angle of 160° or higher.[8-10] This unique surface also tends to make a water droplet to roll over the surface, rather than slide on it, giving the droplet high mobility. With the advances in nano- and micro- electromechanical systems (NEMS and MEMS, respectively) technologies, it is now possible to construct arrays of pillars with a range of shapes, such as triangular spikes,[11,12] hierarchical pillars[13,14] and circular[15,16] and square[17,18] pillars.

The optimal geometry of a textured surface that imparts the highest water repellency to that surface is unclear. More-over, extracting the optimal geometry from trial and error experiments is both expensive and time consuming. In this respect, computer simulations can be useful. In this study, molecular dynamics (MD) simulations were performed to investigate the hydrophobicity of a graphite surface pattern-ed with a periodic array of pillars. This study examined how the contact angle of a water droplet varies according to the width of the pillar and the spacing between neighboring pillars. The effects of the pillar shape were examined by considering parallelepiped and dome-shaped pillars. The mobility of a water droplet on the pillared surface was studied by applying a constant force to an initially static droplet. The results showed that introducing pillars to the graphite surface enhanced the hydrophobicity on the surface, and there was an optimal spacing that gave the highest

hydrophobicity. The dome-shaped pillars enhanced the mobility of the droplet, compared to the parallelepiped pillars.

Simulation Details

A graphite surface, either flat or textured with pillars, was simulated. The flat graphite surface was comprised of 2 layers and 3200 carbon atoms. Two types of pillars on graphite were considered. The first type is a periodic array of parallelepiped pillars, as shown in Figure 1. The height and width of the parallelepiped pillar were varied from 7.2 to 28.8 Å and from 2.13 to 10.65 Å, respectively. The spacing between the neighboring parallelepiped pillars was changed from 2.13 to 10.65 Å. The other type of pillar is a periodic
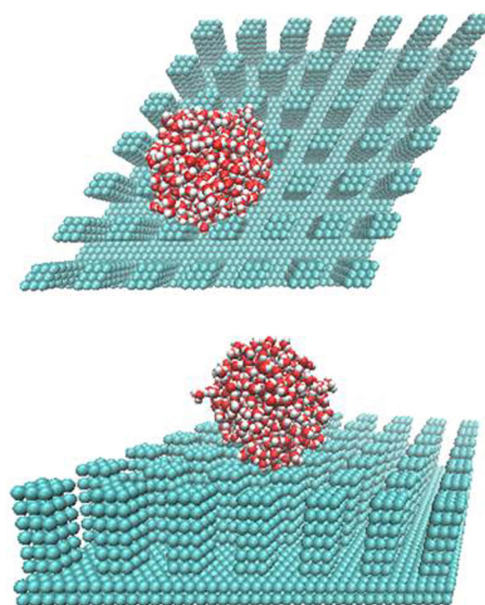

Figure 1. Simulation snapshot of a water droplet on a graphite surface covered with a periodic array of parallelepiped pillars. The top and side views of the droplet are plotted in the top and bottom panels, respectively. The height and width of pillar are 21.6 Å and 6.39 Å, respectively. The wall-to-wall spacing between two neigh-boring pillars is 6.39 Å.
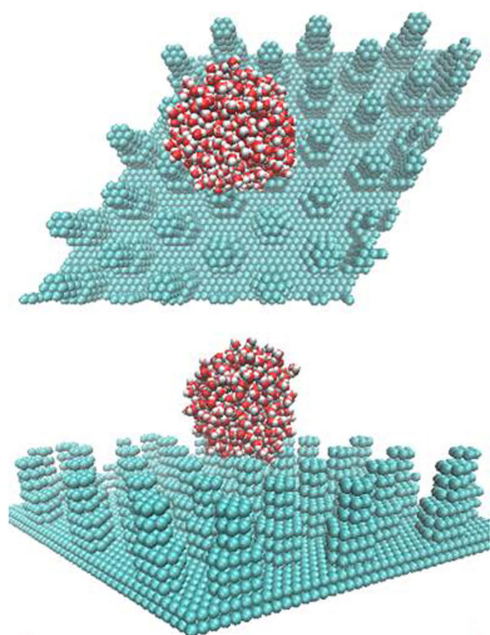
Figure 2. Snapshot of a water droplet on a graphite surface covered with dome-shaped pillars. The height and bottom width of dome are 21.6 Å and 10.64 Å, respectively. The bottom-to-bottom distance between neighboring domes is 6.39 Å.

array of dome-shaped pillars, as shown in Figure 2. The height and width (base diameter) of the dome-shaped pillars was 21.6 and 10.64 Å, respectively. The spacing between the neighboring domes (bottom to bottom distance) was fixed to 8.52 Å.

This study employed the simple point charge (SPC)[19] model, which treats each water molecule as a 3 point charge rigidly bound together (−0.82 and +0.41 on oxygen and hydrogen atoms, respectively).[19] The partial atomic charges interact through the Coulomb potential,

$$U^C(r_{ij}) = \frac{q_i q_j}{4\pi\varepsilon_0 r_{ij}}, \qquad (1)$$

where q_i is the charge on atom i (oxygen or hydrogen), and ε_0 is the vacuum permittivity. r_{ij} is the distance between two atoms i and j. Oxygen atoms interact with themselves through the pairwise Lennard-Jones (LJ) potential,[20]

$$U^{LJ}(r_{ij}) = 4\varepsilon\left[\left(\frac{\sigma}{r_{ij}}\right)^{12} - \left(\frac{\sigma}{r_{ij}}\right)^6\right], \qquad (2)$$

where ε and σ are the LJ energy and length parameters, respectively. The bond distance and angle of the water molecule were fixed using the SHAKE algorithm.[21] The σ and ε values for the oxygen-oxygen interaction were 3.166 Å and 0.1553 kcal/mol, respectively. The Lorentz-Berthelot combination rules[20] were applied to obtain the LJ parameters of the interaction between carbon and oxygen atoms (3.5135 Å and 0.1252 kcal/mol for σ and ε values, respectively). The carbon atoms of the surface are fixed in position. The periodic boundary conditions with a minimum image convention along the direction parallel to the graphite surface

were applied.[20]

The MD simulations are carried out at a fixed temperature of 300 K using the Evans thermostat.[22] The equation of motion was integrated using the leapfrog algorithm with a time step of 1.0 fs. All MD simulations were run for 1 ns using the DL_POLY package.[23]

The contact angle of a water droplet was calculated as follows. For a given snapshot of a droplet, the Z axis was set along the surface normal so that it passes through the center of mass of the droplet. The droplet was then sliced into slabs by binning the Z axis with an equal interval of 2.5 Å. For each slab, the distances of the oxygen atoms from the Z axis, rs, were binned at intervals of 2.5 Å. By averaging more than 300 MD snapshots, the horizontal density profile $\rho(r)|_z$ was calculated for a slab whose Z coordinate was given by z. $\rho(r)|_z$ behaves like a step function of r, which falls from 1.0 g/cm³ to 0 as r increases from zero. The distance at which the density falls below 0.5 g/cm³ is defined as the radius of the droplet at that z value, $r_{drop}(z)$. To do so, $\rho(r)|_z$ was fitted to a hyperbolic tangent function,

$$\rho(r)|_z = \frac{1}{2}(\rho^l + \rho^v) - \frac{1}{2}(\rho^l - \rho^v)\tanh\left(\frac{2(r-r_e)}{d}\right) \qquad (3)$$

where ρ^l and ρ^v are the bulk liquid and vapor densities, r_e is the position of the Gibbs dividing surface and d is the width of the liquid-vapor interface. The Levenberg-Marquardt nonlinear fitting method was used to determine ρ^l, ρ^v, d and r_e.[24]

In Figure 3, r_{drop} was plotted as a function of the height from the surface z. r_{drop} (drawn as circles) was fitted
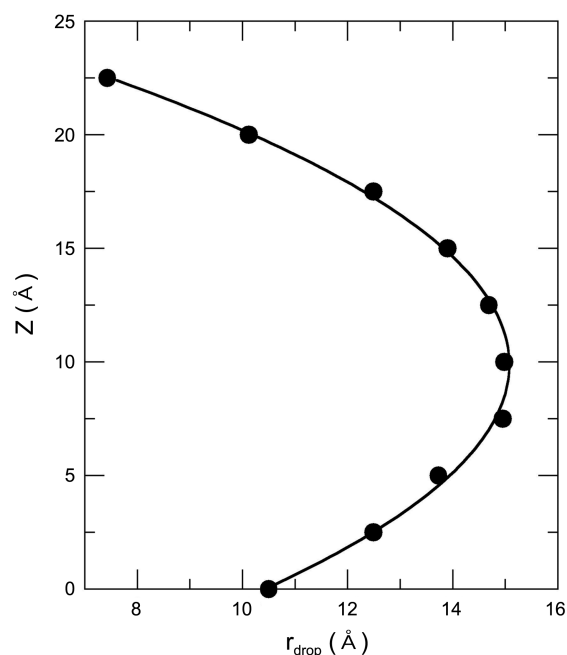

Figure 3. Periphery of a water droplet. Shown is the radius of the droplet r_{drop} as a function of the height from the surface z (circles). Plotted as a solid line is the parabolic fitting function, $r_{drop}(z) = Az^2 + Bz + C$. The water droplet is on top of a graphite surface with parallelepiped pillars with a height and width of 14.4 Å and 4.25 Å, respectively. The spacing between two neighboring pillars is 8.52 Å.

further to a parabolic function of z drawn as a solid line, $r_{drop}(z) = Az^2 + Bz + C$ where A, B and C are constants. The contact angle of a droplet is then given by $\pi/2 + \tan^{-1}(dr_{drop}/dz|_{z=0})$.[25]

Results and Discussion

The contact angle of water droplet on a flat graphite surface did not change significantly as the droplet size was varied: the contact angle changed from 126° to 123° as the diameter of the droplet was decreased from 15 to 27 Å. Presumably, these contact angles will be smaller than those of the macroscopic droplets because the contact angle decreases with decreasing drop size.[26] Given that the contact angle does not depend much on the droplet size, this study examined how the pillar size and shape affect the contact angle by fixing the number of water molecules to 512 (droplet diameter of 27 Å).

The effects of the pillar width on the contact angle were investigated. The width of parallelepiped pillar was varied from 2.13 Å to 10.65 Å, whereas the pillar height and spacing between pillars were fixed to 14.4 Å and 6.39 Å, respectively. Figure 4 shows the contact angle as a function of the pillar width. Note that the contact angles on the surfaces with finite pillar widths are larger than those on the flat surface. Increasing the pillar width, however, did not change the contact angle of the droplet significantly. Presumably, the contact area of the droplet and the vacuum determine the contact angle. Therefore, increasing the pillar width does not change the contact angle provided that the interpillar spacing is fixed. On the other hand, if the pillar width is too small (< 3 Å), the water droplet does not stick to the surface due to the very low contact area of the droplet with the surface. This non-sticking behavior of a droplet for a low contact area with a solid surface was also observed in previous MD simulations.[9]

The effects of varying the spacing between pillars were also examined. The inter-pillar spacing was changed from 0
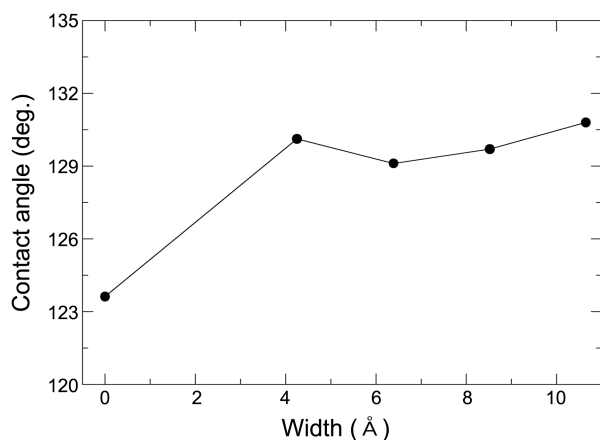

Figure 5. Contact angle as a function of the spacing between neighboring parallelepiped pillars. The line serves as a guide to the eyes. The height and width of the pillar were 14.4 and 4.25 Å, respectively.

to 10.65 Å by fixing the height and width of the pillar to 14.4 and 4.25 Å, respectively. Figure 5 shows that the contact angle varies from 123.6° to 129.8° with increasing spacing from zero to 10.65 Å. The contact angle increased with increasing spacing from zero to 6.39 Å. With further increases in spacing to 10.65 Å, the contact angle decreased to 124.24°. At this large inter-pillar spacing, the water droplet penetrates into the gap between pillars (by 2.61 Å below the top of the pillar). This contrasts with the conventional Cassie-Baxter state of a droplet, where the droplet sits on top of the pillars and does not penetrate into the gap between the pillars. This penetration is characteristic of the Wenzel state where the droplet completely fills in the gap between the pillars. As a result, the surface is less hydrophobic and the contact angle decreases. In summary, Figure 5 shows that there is an optimal inter-pillar spacing (6.39 Å) that gives rise to the maximum hydrophobicity.

Finally, this study examined a graphite surface covered with dome-shaped pillars, 21.6 and 10.64 Å in height and base diameter, respectively. For comparison, a similar surface patterned with parallelepiped pillars (the height and bottom diameter are 21.6 and 10.64 Å, respectively) was simulated. The spacing between two neighboring pillars was kept the same (6.39 Å) for both dome-shaped and parallelepiped pillars. The contact angle for the dome-covered surface (129.2°) was slightly higher than that of the surface with parallelepiped pillars (127.7°). The mobility of a water droplet on both surfaces was further investigated. A constant external force was applied to the static droplet in the direction parallel to the surface (along the X axis), which allowed the droplet to move as a whole over the surface. The strength of the external force was varied continuously to determine the minimum force required to move the water droplet. On the dome-covered surface, 0.028 nN is needed to move the water droplet. On the surface with parallelepiped pillars, the minimum force was found to be 0.04 nN, which is 0.012 nN higher than that of the dome-covered surface. Therefore, the mobility of a water droplet was higher over

Figure 4. Contact angle *vs.* pillar width. The width of parallelepiped pillar was varied as 4.25, 6.39, 8.52, and 10.65 Å. The width of 0 corresponds to a flat surface. The pillar height and spacing between neighboring pillars were fixed to 14.4 Å and 6.39 Å, respectively.
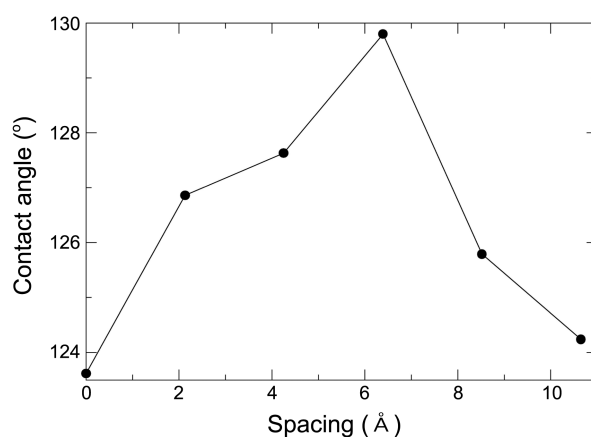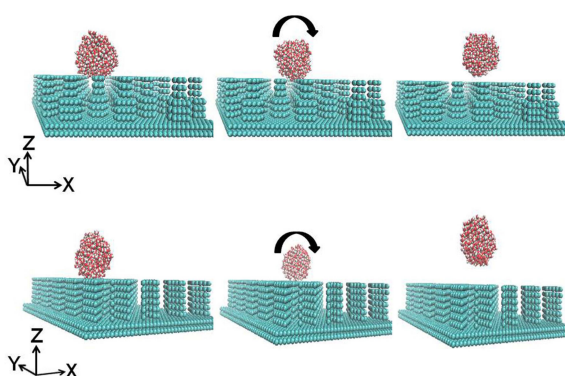
Figure 6. Mobility of a water droplet on a pillared surface. The top (bottom) panel shows the snapshots of a water droplet moving on the dome-shaped (parallelepiped) pillars. In each panel, the left snapshot (top and bottom) shows the initial state of the droplet; the middle shows the rolling motion of droplet; the right (top and bottom) illustrates the water droplet taking off from the surface. An external force was applied along the *X* direction.

the dome-covered surface. Above the threshold value of the external force, the water droplet rolled over the surface and then left the surface. In contrast, the water droplet on the flat surface slid over the surface, instead of rolling. Therefore, the presence of an interpillar gap causes the droplet to roll.

Summary

Molecular dynamics simulations were performed to examine the hydrophobicity of a graphite surface covered with pillars. The contact angle of a water droplet was investigated at different pillar widths and gaps between pillars. The results suggested that a surface with pillars, regardless of whether it is parallelepiped or dome shaped, is more hydrophobic than a flat surface, giving rise to a higher water contact angle. An optimal spacing between pillars that gives the highest water contact angle was found. Dome shaped pillars give rise to enhanced mobility of water droplet on the surface compared to parallelepiped pillars. The presence of pillars makes the droplet roll instead of sliding, which was observed in the case of a flat surface.

References

1. Nakajima, A.; Hashimoto, K.; Watanabe, T.; Takai, K.; Yamauchi, G.; Fujishima, A. *Langmuir* **2000**, *16*, 7044.
2. Michielsen, S.; Lee, H. J. *Langmuir* **2007**, *23*, 6004.
3. Feng, L.; Li, S.; Li, Y.; Li, H.; Zhang, L.; Zhai, J.; Song, Y.; Liu, B.; Jiang, L.; Zhu, D. *Advanced Materials* **2002**, *14*, 1857.
4. He, B.; Lee, J.; Patankar, N. A. *Colloids and Surfaces A: Physico-chemical and Engineering Aspects* **2004**, *248*, 101.
5. Hyväluoma, J.; Timonen, J. *Journal of Statistical Mechanics: Theory and Experiment* **2009**, *2009*, P06010.
6. Patankar, N. A. *Langmuir* **2004**, *20*, 8209.
7. Tuteja, A.; Choi, W.; Ma, M.; Mabry, J. M.; Mazzella, S. A.; Rutledge, G. C.; McKinley, G. H.; Cohen, R. E. *Science* **2007**, *318*, 1618.
8. Kantesh, B.; Ruben Galiano, B.; Debrupa, L.; Arvind, A. *Nanotechnology* **2009**, *20*, 305707.
9. Lundgren, M.; Allan, N. L.; Cosgrove, T. *Langmuir* **2006**, *23*, 1187.
10. Seung-Mo, L.; Tai Hun, K. *Journal of Micromechanics and Microengineering* **2007**, *17*, 687.
11. Narhe, R. D.; Beysens, D. A. *EPL (Europhysics Letters)* **2006**, *75*, 98.
12. Lafuma, A.; Quere, D. *Nat Mater* **2003**, *2*, 457.
13. Bok, H.-M.; Kim, S.; Yoo, S.-H.; Kim, S. K.; Park, S. *Langmuir* **2008**, *24*, 4168.
14. Ho, A. Y. Y.; Yeo, L. P.; Lam, Y. C.; Rodriiguez, I. *ACS Nano* **2011**, *5*, 1897.
15. Martines, E.; Seunarine, K.; Morgan, H.; Gadegaard, N.; Wilkinson, C. D. W.; Riehle, M. O. *Nano Letters* **2005**, *5*, 2097.
16. Nosonovsky, M.; Bhushan, B. *Nano Letters* **2007**, *7*, 2633.
17. Dorrer, C.; Rühe, J. *Langmuir* **2006**, *22*, 7652.
18. Narhe, R. D.; Beysens, D. A. *Langmuir* **2007**, *23*, 6486.
19. Berendsen, H. J. C.; Postma, J. P. M.; Gunsteren, W. F. V.; Hermans, J. In *Intermolecular Forces*; Pullmann, B., Ed.; Reidel Publishing Company: Dordrecht, 1981; p 331.
20. Allen, M. P.; Tildesley, D. J. *Computer Simulation of Liquids*; Claredon Press: Oxford, 1987.
21. Miyamoto, S.; Kollman, P. A. *Journal of Computational Chemistry* **1992**, *13*, 952.
22. Evans, D. J.; Morriss, O. P. *Computer Physics Reports* **1984**, *1*, 297.
23. Smith, W.; Yong, C. W.; Rodger, P. M. *Molecular Simulation* **2002**, *28*, 385.
24. Marquardt, D. *J. Soc. Ind. Appl. Math.* **1963**, *11*, 431.
25. Giovambattista, N.; Debenedetti, P. G.; Rossky, P. J. *The Journal of Physical Chemistry B* **2007**, *111*, 9581.
26. Good, R. J.; Koo, M. N. *Journal of Colloid and Interface Science* **1979**, *71*, 283.